

Treatment of SPR background in Total internal reflection ellipsometry. Characterization of RNA polymerase II films formation.

Dušan Hemzal^{1,2}, Yu Ri Kang³, Jan Dvořák¹, Tomasz Kabzinski², Karel Kubiček², Young Dong Kim³ and Josef Humlíček^{1,2}

Abstract

To deal with the general problem of biomolecules specific binding analysis, we have applied the technique of difference spectra to the SPR-enhanced Total internal reflection ellipsometry measurement. We suggest a three-step treatment of the SPR background, that can easily be integrated with usual measurement routine. First, making use of the difference spectrum in ellipsometric angle Δ , single peak footprints of the topmost layer are obtained that facilitate its sensitive detection during the film growth. Subsequently, circumventing the need of explicit knowledge of the substrate properties, the difference spectra peaks can be used for the end-point analysis of binding. Finally, tracking the binding effectivity of the analyte we determine the injection speed and analyte concentration windows needed for successful monitoring of the film growth. We demonstrate our approach on a comprehensive two-stage binding experiment involving two biologically relevant molecules: the C-terminal domain of RNA polymerase II and CID of one of its transcription factors, the Rtt103 protein.

Keywords

Spectroscopic Ellipsometry, Surface plasmon resonance, TIRE, RNA polymerase II, CTD, Rtt103

Introduction

Adsorption of a thin bio-molecular film on the substrate produces small changes in the measured optical spectra. In plasmonics,¹ these changes can be highly enhanced using substrates that exhibit surface plasmon resonance (SPR). Combining SPR² with spectroscopic ellipsometry³ in total internal reflection setting (TIRE) results in SPR-TIRE,⁴ which surpasses conventional SPR techniques by additional information on the reflection induced phase-shifts. Contained in the ellipsometric angle Δ , this information is responsible for the high sensitivity of SPR-TIRE.⁵ The usual angle-scanned reflectance is also accessible in SPR-TIRE measurement: it is related to the ellipsometric angle Ψ , albeit it is customary to perform wavelength scan in ellipsometry.

In both SPR and SPR-TIRE, the contribution from the film is highly enhanced by the resonance in a metallic layer within the substrate. In consequence, both techniques must cope with high sensitivity to substrate quality. When the requirement of SPR is withdrawn, leaving only TIRE, non-metallic substrates can be used⁶ and other measurement modalities are available^{7,8} at the expense, however, of lower sensitivity compared to SPR-TIRE (in correspondence with usual practice, we will omit SPR- in further).

In Kretschmann configuration the TIRE substrate usually consists of a wavefront coupling prism followed by the TIRE chip (see Fig. 1), attached to the prism using an index-matching immersion oil. The TIRE chip itself consists of a (glass) slide with SPR-active metal layer and possible additional self-assembled mono-layers (SAMs), intended to facilitate immobilization of the host molecules. Although air

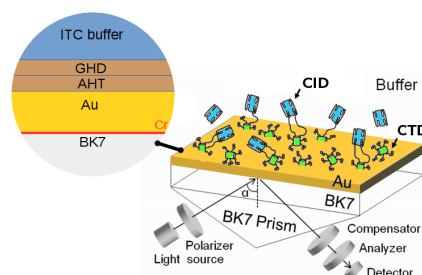


Figure 1. Schematic view of the TIRE experiment setup. The host, immobilized to the TIRE chip, is accessed by the buffer dispersed analyte. The TIRE chip is attached to a glass prism using immersion oil; detail of the active surface including the immobilization facilitating monolayers is shown.

ambient measurements are possible, a small-volume flow cell is usually clamped to the substrate and flushed with liquid buffer. Consequently, micro-fluidic setup can be used to inject the analyte through the cell.

¹Dept. condensed matter physics, Masaryk University, Kotlářská 2, 611 37 Brno, Czech Republic

²CEITEC - Central European Institute of Technology, Masaryk University, Kamenice 753/5, 625 00 Brno, Czech Republic

³Nano-Optical Property Laboratory and Department of Physics, Kyung Hee University, Seoul 130-701, Republic of Korea

Corresponding author:

Dušan Hemzal, Dept. condensed matter physics, Masaryk University, Kotlářská 2, 611 37 Brno, Czech Republic

Email: hemzal@physics.muni.cz

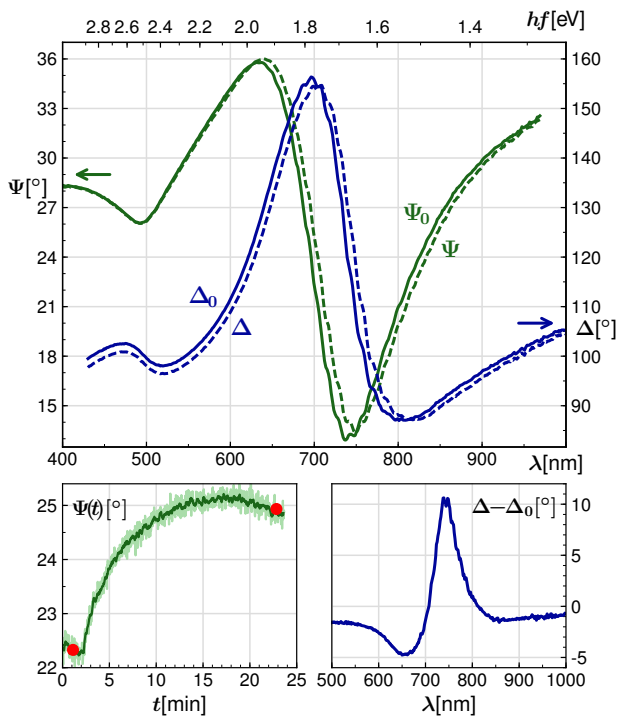


Figure 2. Ellipsometric spectra from TIRE measurement (upper panel) taken at the angle of incidence 70° with bare TIRE chip (Ψ_0 , Δ_0 , solid lines) and after immobilization of CTD (Ψ , Δ , broken lines) sample (ch8_1, see Tab. 1). Lower panels: selection from dynamic monitoring of Ψ (at 701 nm) during injection of the CTD (left); diamonds mark times when the full spectra in the main plot were taken. The corresponding difference spectrum $\Delta - \Delta_0$ (right) for these two times.

After submersion of the substrate in buffer, background measurement is recorded revealing the characteristic resonance structure. During the analyte injection induced film growth over the substrate, the ellipsometric spectrum is modified by small shift of the resonance structure and change of its depth (cf. Fig. 2). The kinetics of these changes has been studied, resulting in estimate of the binding constant K_d from a TIRE experiment.^{9,10}

As a rule, the model of the substrate is established first with thicknesses fitted from the background measurement. The acquired values are carried over to the sample measurement, where only the parameters of the film are fitted. The main problems in quantitative analysis of TIRE experiments thus come from the imperfection (including interfaces roughness and over-layers), and especially from the metallic layer, needed to invoke the plasmonic resonance, itself.

For the metallic layer we used gold, whose thickness for optimal performance (approx. 50 nm¹¹) lies well above the threshold of about 1.5 nm, when the layers already exhibit bulk properties.¹² On the other hand, the resonance in water ambient is observed near 1.7 eV, ie. below the inter-band transition threshold of gold. In this region, the Drude contribution of free electrons is very sensitive to gold layer quality (primarily the grain size and surface roughness¹³), producing high spread in optical constants obtained from measurement on different samples.

In addition, correlation between thickness and refractive index of the measured film, see (6), cannot be suppressed

using broad spectral measurements, because in SPR only narrow spectral range near the resonance provides sufficient sensitivity. Hence, unless the thickness is measured independently (eg. by inclusion of QCM¹⁴), it would be desirable to avoid explicit fitting of the data.

For samples with high homogeneity, the preferred technique for analysis of the layer growth might be the virtual interface method.¹⁵ Having, however, in mind the complications connected with the TIRE chip, as well as the stochastic nature of biological layers, we will, instead, use the fact that the forming film is thin and use Taylor expansion to study the contribution caused by injection of the analyte via difference spectra.

We demonstrate our procedure on a two-stage binding experiment: first, we study immobilization of various modifications of C-terminal domain (CTD) of RNA Polymerase II (RNAPII), RNAPII-CTD. Subsequently, we study binding of the CTD interacting domain (CID) of the Rtt103 protein, Rtt103-CID, to the immobilized CTD.

Theory

Explicit fits of real-world layered structures from ellipsometric measurements will unavoidably be hindered by significant correlation of the fitted parameters. On the other hand, recording independently the background and sample spectra, one can certainly combine them into a difference spectrum. Constituting a discrete version of the derivative, the difference spectrum should emphasize the changes caused by analyte injection, thus facilitating its detection.

Generic behavior of the difference spectra can be demonstrated from the measured curves in Fig. 2. Considering red-shifting of the resonance dip with analyte injection, difference in Ψ will show a maximum $\bar{\Psi}_{\max}$ followed by a minimum, while difference in Δ will be dominated by a single maximum $\bar{\Delta}_{\max}$. Close to the resonance, the difference in Ψ will cross zero whereas difference in Δ will exhibit the maximum $\bar{\Delta}_{\max}$, cf. also Fig. 6. As a result, if a single quantity should be used to monitor the film growth, the best sensitivity is reached using the values of the difference spectra maxima, especially $\bar{\Delta}_{\max}$ as supported also below.

Of course, prior to extracting any information from the difference spectra it is necessary to study their properties and justify the application of the subtraction. We will inspect the difference spectra against their linear expansion: numerical reliability of the difference spectra requires the error of such an approximation to vanish for layers of negligible thickness.

For description of the light propagation through the layered structures in question we use the matrix formalism.¹⁶ The electric amplitudes of transmitted (E_t) and reflected (E_r) field are connected to the incident (E_i) one through the propagation matrix \mathbf{P} ,

$$\begin{bmatrix} E_i \\ E_r \end{bmatrix} = \mathbf{P} \begin{bmatrix} E_t \\ 0 \end{bmatrix}, \quad (1)$$

where

$$\mathbf{P} = (\mathbf{V}_0)^{-1}(\mathbf{R}_1)^{-1} \dots (\mathbf{R}_m)^{-1}\mathbf{V}_f. \quad (2)$$

Central to the matrix formalism is the inverse of the propagation matrix \mathbf{R}_j in the j -th layer,

$$\mathbf{R}_j^{-1} = \begin{pmatrix} \cos \theta_j & -\frac{\sin \theta_j}{\tilde{n}_j} \\ -\tilde{n}_j \sin \theta_j & \cos \theta_j \end{pmatrix}, \quad (3)$$

where θ_j is the phase shift acquired by propagation across this layer. The definition of the effective index of refraction \tilde{n}_j and interface matrices \mathbf{V} is polarization dependent; for complete notation see the Supplement.

As customary in SPR analysis, the media are listed from the wavefront coupling prism (starting with index 0) through the substrate up to the ambient (with index f) and the light impacts from the ambient.

To address the effect of the top-most layer in the system, the propagation matrix of the substrate can be factorized as $\mathbf{P} = \mathbf{B}\mathbf{V}_f$, where

$$\mathbf{B} = \mathbf{V}_0^{-1}\mathbf{R}_1^{-1} \dots \mathbf{R}_l^{-1} \equiv \begin{pmatrix} a & b \\ c & d \end{pmatrix}; \quad (4)$$

to distinguish the polarization we will use subscripts s and p . Subsequently, a TIRE chip submersed in an ambient with refractive index n_f produces the substrate-related reflectivity ratio $\rho_0 = r_{0p}/r_{0s}$ where the reflectivities

$$\begin{aligned} r_{0p} &= (d_p n_f + c_p \cos \phi_f) / (b_p n_f + a_p \cos \phi_f) \\ r_{0s} &= (c_s + d_s n_f \cos \phi_f) / (a_s + b_s n_f \cos \phi_f) \end{aligned} \quad (5)$$

are reached using (1) and (4) with ϕ_f being the angle-to-normal of light transmitted into ambient. The reflectivity ratio decouples into substrate-related ellipsometric angles through $\rho_0 = \tan \Psi_0 \cdot \exp(i\Delta_0)$.

A thin layer of thickness t and refractive index n (with the light transmitted into this layer at angle ϕ) can be approximately described by the matrix $(\mathbf{R}^{-1})_{\text{thin}} \equiv \mathbf{S}$, with

$$\mathbf{S} \approx \begin{pmatrix} 1 & -\frac{i}{\tilde{n}} \frac{2\pi}{\lambda} n t \cos \phi \\ -i\tilde{n} \frac{2\pi}{\lambda} n t \cos \phi & 1 \end{pmatrix}, \quad (6)$$

where we have used the lowest-order Taylor expansion in t/λ . Adding this layer on the substrate, the overall propagation matrix becomes $\mathbf{B}\mathbf{S}\mathbf{V}_f$, producing the sample-related ellipsometric angles Ψ and Δ . Typical behavior of a BK7/Au/water system is shown in Fig. 3; in all simulations, optical constants of gold from¹⁷ were used.

Combining substrate and sample measurements, one can find their difference

$$\begin{aligned} \Psi - \Psi_0 &\approx 2\pi \text{Im} \left\{ \frac{A}{A_0} - \frac{E}{E_0} \right\} \frac{|\rho_0|}{1 + |\rho_0|^2} \frac{t}{\lambda} \\ \Delta - \Delta_0 &\approx -2\pi \text{Re} \left\{ \frac{A}{A_0} - \frac{E}{E_0} \right\} \frac{t}{\lambda}, \end{aligned} \quad (7)$$

where

$$\begin{aligned} A &= (d_p n^2 \cos \phi_f + c_p n_f \cos^2 \phi)(a_s + b_s n_f \cos \phi_f) + \\ &+ (b_s n^2 \cos^2 \phi + a_s n_f \cos \phi_f)(d_p n_f + c_p \cos \phi_f) \\ E &= (b_p n^2 \cos \phi_f + a_p n_f \cos^2 \phi)(c_s + d_s n_f \cos \phi_f) + \\ &+ (d_s n^2 \cos^2 \phi + c_s n_f \cos \phi_f)(b_p n_f + a_p \cos \phi_f) \end{aligned} \quad (8)$$

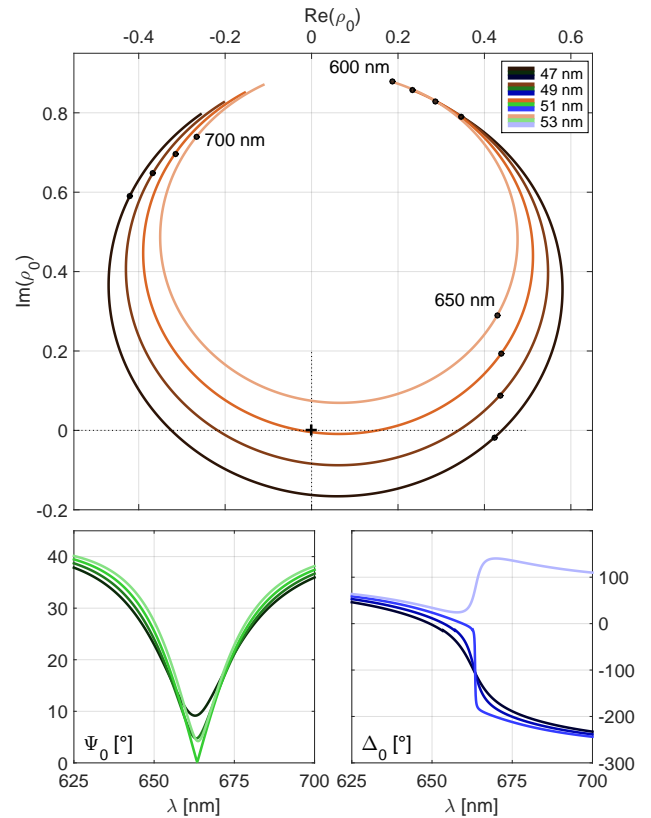


Figure 3. Simulation of the spectral dependence at AOI 70° (wavelength runs along the curves) of complex reflectance ratio ρ_0 for Au over BK7 system in water ambient (top) with different thicknesses of gold layer (as noted in the legend). Bottom panels: spectral dependence of Ψ_0 and Δ_0 , as calculated from ρ_0 ; note the different behavior of Δ when ρ_0 encircles the origin (emphasized by a cross) and when it doesn't.

and we have, for convenience, used factorization of ρ_0 different from the physical one in eq. (5). Namely, we have put $\rho_0 = A_0/E_0$, where

$$\begin{aligned} A_0 &= (d_p n_f + c_p \cos \phi_f)(a_s + b_s n_f \cos \phi_f) \\ E_0 &= (b_p n_f + a_p \cos \phi_f)(c_s + d_s n_f \cos \phi_f). \end{aligned} \quad (9)$$

For details on derivation of eqs. (6) and (7) see the Supplement.

Equation (7) can be viewed as ellipsometric counterpart to classical SPR reflectivity formulas¹⁸ and used for direct simulation of the difference ellipsometric spectra. As long as the layers in question are much thinner than the wavelength of light, formulas (7) should provide reasonable description of the growing film contribution: they can even be used turn by turn for step-wise deposition or describe non-compact layers using effective medium approach (for importance of this fact see also Fig. 10).

The linear approximation will fail in regions where the first-order coefficients approach zero and higher-order terms become prominent, as will commonly happen close to the resonance, cf. Fig. 4. This effect, dominant especially in numerical simulations with fixed parameters, will be less important in real measurement due to the smearing effect of the spread in angle of incidence and/or wavelength.

To this end, we have performed a multi-parametric simulation of the approximation error, whose results are

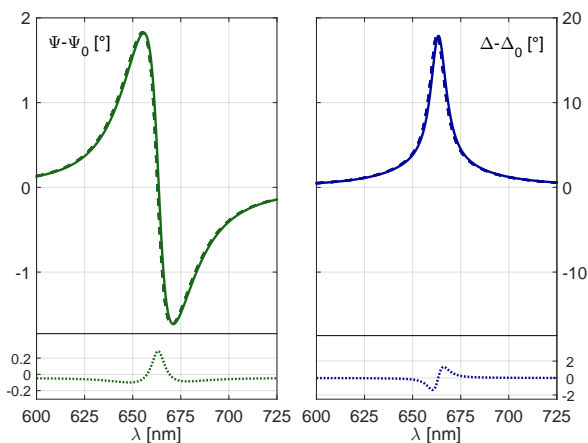


Figure 4. Comparison of numerically simulated difference spectra (solid lines) and prediction by formulas (7) (broken lines). The film was 1 nm of $n = 1.4$ material over 47 nm of Au over BK7 substrate, with AOI 70° . Left panels: $\Psi - \Psi_0$, right panels: $\Delta - \Delta_0$. The bottom panels show explicitly the approximation error. Note the different vertical ranges in the panels.

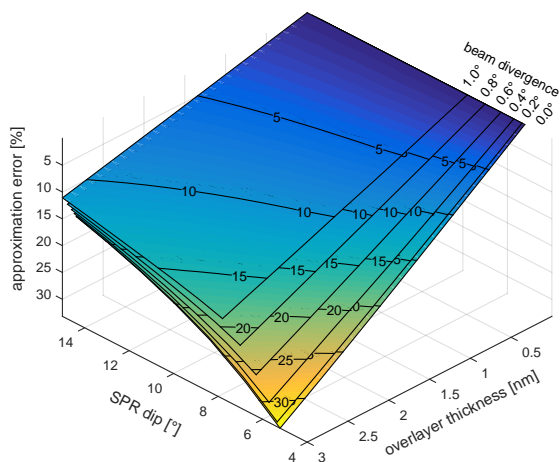


Figure 5. Multi-parametric simulation of difference spectra stability. Dependence of the linear approximation error in $\Psi - \Psi_0$ on substrate resonance depth and thickness of the growing layer is given for several values of beam divergence and overlayer with $n = 1.4$; wavelength smearing was set to $\Delta\lambda = 4$ nm.

summarized in Fig. 5. As the figure confirms, when wavelength smearing due to monochromator (we have chosen $\Delta\lambda = 4$ nm) and beam divergence due to focusing optics are considered in simulation, the approximation errors stay at acceptable levels.

Plots of the type of Fig. 5 provide a quick check of the difference spectra reliability, based on user accessible parameters: depth of substrate resonance dip (available from background measurement), growing layer thickness (related to analyte size) and beam divergence (depending on focussation used). In our experience, the error of order 10-15% is acceptable, especially due to low coverage of the substrate observed in the measurements. Above this threshold, the error becomes comparable with uncertainty produced due to the noise in measured signals, and the

conclusions inferred from the difference spectra may become unrealistic.

Measurement and results

In our previous work we reported on TIRE measurement of 5'-AGCT-3' oligomer unspecific binding to HSA attached over the Au surface of the SPR chip,¹⁹ which resulted in estimation of the spectral dependence of optical constants of the protein used, and on *in situ* monitoring of the specific binding between EGRF protein and EGRF aptamer.²⁰ The binding constant between EGFR and its aptamers is reported in the nanomolar range.²¹ We now report on substantially weaker specific binding experiment using RNAPII-CTD and Rtt103-CID: we immobilize various modifications of short (E2) and long (E213 and E513) repeats of CTD over two-step prepared SAMs and, subsequently, we study the binding of the Rtt103-CID to the immobilized CTD (for details on the samples and chemistry see Appendix).

Transcription by RNAPII is tightly coupled to majority of pre-mRNA processing steps. The CTD forms a flexible tail of RNAPII and serves as a binding platform for various co-transcriptional processing factors. There are only few structures available for processing factors bound to the modified CTD, for example.²² Structure determination of these complexes is challenging because of the weak and ultra-weak protein-protein interactions ($K_d \geq 10^{-4}$ M) involved. This weak interactions are undetectable by most biochemical methods, but SPR techniques seem to constitute a feasible alternative.¹⁰

TIRE spectra. Ellipsometric angles Ψ , Δ were recorded during the binding experiment at room temperature with Woollam M2000 multi-channel ellipsometer in the spectral range 400–1600 nm using auto-retarder. The ellipsometer arms were set to AOI 70° and (semi)half cylinder prism was used with focussation probes. The TIRE liquid transport system consisted of a liquid cell with three separate channels with the volume of 80 μ l each, a 2.5 ml degasser to remove residual gas in the liquid, and a syringe pump to control the liquid flow rate. At the beginning of each measurement, buffer was injected to rinse the selected channel for several minutes at 100 μ l/min. Altogether, 13 independent channels across 5 different TIRE chips were used during measurements, as summarized in Tabs. 1,2.

In the first experiment, injection of 500 μ l of the diluted CTD peptides took place at the nominal flow speed of 100 μ l/min for 25 minutes, covering transport of the sample towards the cell, the intrinsic injection and final rinsing of the cell with buffer. Having reached an equilibrium, a full spectroscopic measurement (300 analyzer revolutions) was taken. Second, similar experiment took place keeping the flow speed of 100 μ l/min for the first 3 minutes to transport the sample towards the cell only, followed directly by the intrinsic injection at 20 μ l/min until minute 25 of the injection.

Finally, directly following the 20 μ l/min CTD immobilization, 200 μ l of diluted Rtt103-CID were injected in a rising concentration sequence at 50 μ l/min, followed always by slow rinsing by buffer at the same flow speed (cf. Fig. 9). After the final sample (at nominal concentration of the

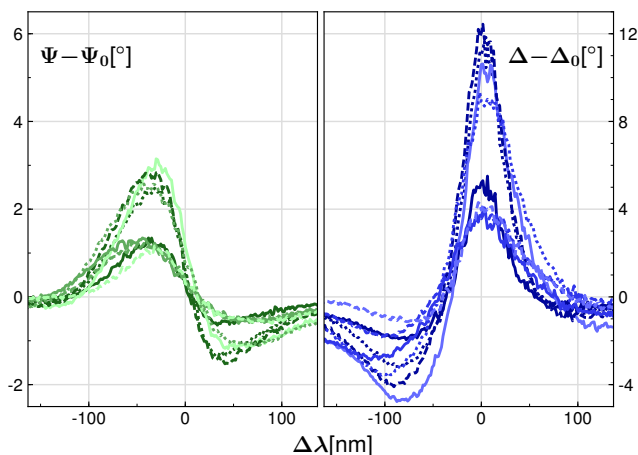


Figure 6. Difference spectra in Ψ (left panel) and Δ (right panel), for flow speed $20 \mu\text{l}/\text{min}$ (cf. Tab. 1); dark to light: ch6 to ch8, solid to dotted: .1 to .3 (see also Tab. 2). The spectra from different substrates were aligned relative to wavelength of resonance (in Ψ_0) to isolate the contribution from different concentration of CTD. Note the different vertical scale in the panels.

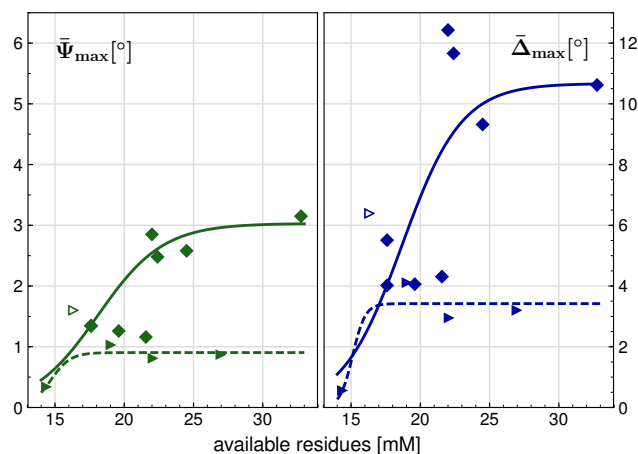


Figure 7. Binding effectivity in Ψ (left panel) and Δ (right panel) for $20 \mu\text{l}/\text{min}$ (diamonds, solid line for fit) and $100 \mu\text{l}/\text{min}$ (triangles, dashed line for fit); cf. Tabs. 1, 2. The outliers (open symbols) were excluded from fits.

available Rtt103-CID), a full spectroscopic measurement was taken. Changes of the optical properties near the metal surface during each binding step were monitored at selected wavelengths (16 wavelengths between 701-796 nm, 10 analyzer revolutions each) near the SPR resonance using the real-time modality of the Woollam system (WVase 3.774).

Prior to recording any data, the reproducibility and SAM control measurements were successfully passed.

CTD immobilization. In each experiment, the background (Ψ_0 and Δ_0 , with buffer in the cell only) was recorded, which allows to form the difference spectra $\bar{\Psi} \equiv \Psi - \Psi_0$ and $\bar{\Delta} \equiv \Delta - \Delta_0$ (cf. Fig. 6 for flow speed $20 \mu\text{l}/\text{min}$) after the analyte injection. Consequently, we extract the peak values $\bar{\Psi}_{\text{max}}$ and $\bar{\Delta}_{\text{max}}$ from the difference spectra and plot them

Table 1. CTD immobilization, for flow $100 \mu\text{l}/\text{min}$.

code	peptide	concentration [μM]	$\bar{\Psi}_{\text{max}}$ [$^\circ$]	$\bar{\Delta}_{\text{max}}$ [$^\circ$]
ch4_1	E2 AB	333	1.60	6.39
ch4_3	E2 C	293	0.34	0.56
ch5_1	E2 AC	450	0.81	2.95
ch5_2	E2 BC	550	0.87	3.20
ch5_3	E2 AD	388	1.03	4.11

Table 2. CTD immobilization, for flow $20 \mu\text{l}/\text{min}$.

code	peptide	concentration [μM]	$\bar{\Psi}_{\text{max}}$ [$^\circ$]	$\bar{\Delta}_{\text{max}}$ [$^\circ$]
ch6_1	E2 C	352	1.34	5.51
ch6_2	E2 CD	440	2.85	12.43
ch6_3	E213fl	192	2.48	11.66
ch7_1	E2 C	352	1.35	4.02
ch7_2	E2 AB	400	1.26	4.06
ch7_3	E2	490	2.58	9.32
ch8_1	E513fl	280	3.15	10.62
ch8_2	E2 CD	440	1.16	4.31

Table 3. Sigmoid fitting of CTD immobilization.

	flow [$\mu\text{l}/\text{min}$]	A [$^\circ$]	Q	B [μM^{-1}]	M [mM]
$\bar{\Psi}_{\text{max}}$:	20	3.03	1.46	0.425	17.2
	100	0.91	0.10	1.421	16.3
$\bar{\Delta}_{\text{max}}$:	20	10.67	1.98	0.464	17.2
	100	3.42	6.09	2.224	14.3

against the number of available residues in each experiment; we define the latter as the concentration of the given injection times the number of amino acids per peptide at the given injection speed (cf. Fig. 7). The construction of the available residues respects the fact that optical response (i.e. refractive index) change due to the growing film is proportional to the overall amount of material deposited.

Using the data from full spectroscopic measurements, both $100 \mu\text{l}/\text{min}$ and $20 \mu\text{l}/\text{min}$ immobilizations are summarized in Tabs. 1 and 2, respectively, together with the extracted maxima:

To link the dependence of ellipsometric response obtained in Fig. 7 to the available residues, we use for fitting of the both ellipsometric angles difference maxima a (sub)family of generalized sigmoids with the lower asymptote fixed to zero (ie $\bar{\Psi}_{\text{max}} = \bar{\Delta}_{\text{max}} = 0$ at no binding). The generic form for such a sigmoid reads

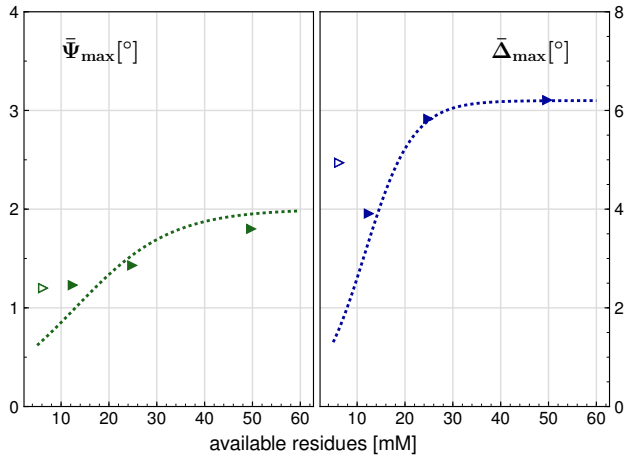
$$\sigma(x) = \frac{A}{1 + Qe^{-B(x-M)}}, \quad (10)$$

where x stands for the amount of available residua in our case, A has the meaning of asymptotic response to the added layer and M is the concentration with highest derivative of response change. The results of the fits are summarized in Tab. 3:

CID binding. To demonstrate the utility of the suggested treatment we have monitored the second stage of our binding experiment using the dynamic spectrum only. Usually, the best sensitivity wavelengths for Ψ and Δ are unknown in advance, so the binding is monitored on several wavelengths near the background plasmon resonance. Such data (in our case the wavelengths in the range 701-796 nm, with 6 nm step) are, however, already sufficient to locate $\bar{\Psi}_{\text{max}}$ and $\bar{\Delta}_{\text{max}}$. The results of the analysis are summarized in Tab. 4:

Table 4. Rtt103 binding over E2C (ch7_1) at 50 $\mu\text{l}/\text{min}$.

code	concentration [μM]	$\bar{\Psi}_{\text{max}}$ [$^{\circ}$]	$\bar{\Delta}_{\text{max}}$ [$^{\circ}$]
1/8	44	1.20	4.94
1/4	88	1.23	3.91
1/2	175	1.43	5.83
1/1	350	1.80	6.21

**Figure 8.** Binding results analysis of Rtt103 at 50 $\mu\text{l}/\text{min}$ (cf. Tab. 4). The lines are guide to the eye (with outliers in open symbols).

The highest derivative of the sensitivity to Rtt103 injection appears for selected injection speed around 100 μM protein concentration.

As a supplementary result we provide an estimate of the binding constant of Rtt103/CTD interaction.

The equilibrium conditions of the reaction $\text{H} + \text{G} \leftrightarrow \text{C}$ are characterized by the reaction dissociation constant K_d . We will denote concentration by square bracket, in particular we use $[\]^0$ and $[\]^\infty$ for initial and equilibrium values, respectively. Then, in case of 1:1 binding the concentrations constraint reads $[\text{C}](t) + [\text{H}](t) = [\text{H}]^0$, because every produced molecule of the product C depletes the initial host abundance $[\text{H}]^0$. If, in addition, the concentration of analyte G is kept constant, $[\text{G}](t) \equiv [\text{G}]^0$ (eg. using a flow cell such as in a TIRE experiment), the change of the product concentration in the course of time is expected in the form

$$[\text{C}](t) - [\text{C}]^\infty = ([\text{C}]^0 - [\text{C}]^\infty) e^{-\alpha t}, \quad (11)$$

where

$$[\text{C}]^\infty = \frac{[\text{H}]^0[\text{G}]^0}{[\text{G}]^0 + K_d} \quad (12)$$

is the asymptotic concentration of the product and

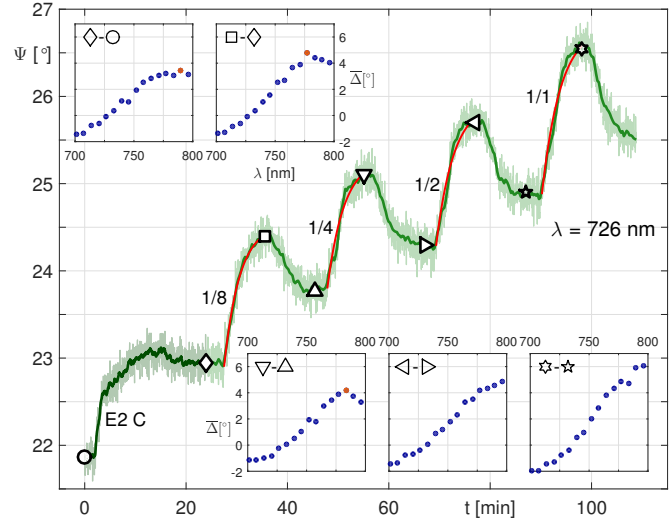
$$\alpha = -[\text{G}]^0 k_{\text{on}} + k_{\text{off}}, \quad (13)$$

where $K_d = k_{\text{off}}/k_{\text{on}}$.

Since the exponent αt is dimensionless, it is preferable to fit the binding constant from α . To perform such fit, time-dependence of any observable is sufficient and the (often cumbersome) relationship between concentration and the measured quantity need not be studied. We will use a simplified version of this approach to process the

Table 5. Evaluation of Rtt103 binding constant to E2 C peptide (ch7_1).

code	$[\text{C}]^0$ [μM]	$[\text{C}]^\infty$ [μM]	α [min^{-1}]	K_d [μM]
1/8	24.60	26.80	0.271	681
1/4	24.03	25.94	0.288	1506
1/2	23.63	25.29	0.304	1823
1/1	22.91	24.53	0.330	

**Figure 9.** Kinetic study of Rtt103-CID binding over E2 C peptide (ch7_1) using maximum sensitivity wavelength in Ψ . First part of the curve maps E2 C immobilization, the four Rtt103-CID binding steps follow (light) with fits of the association phase depicted (orange); see Tab. 5 for details. At marked instants, full spectra were taken and the resulting difference spectra in Δ are given in the insets together with highlighting $\bar{\Delta}_{\text{max}}$, where encountered.

measured data plotted in Fig. 9; the non-covalent character of the studied protein-protein interaction is evident. Taking two successive injections of the analyte with comparable concentrations $[\text{G}]_1$ and $[\text{G}]_2$, the dissociation constant can be considered constant and estimated from (13) as

$$K_d = \frac{\alpha_1[\text{G}]_2 - \alpha_2[\text{G}]_1}{\alpha_2 - \alpha_1}. \quad (14)$$

The results of the Rtt103-CID binding fits (11) and resulting values of K_d using (14) are summarized in Tab. 5.

Discussion

Difference spectra. When monitoring the growing layer, the SPR dip can happen to move across the selected wavelength, accompanied by a minimum in p-polarized reflectivity (and, hence, in Ψ). Combining the sample and reference channel, the analyte dependent zero-crossing point of the difference SPR spectrum can be calibrated with high precision.²³

In ellipsometry, the SPR dip crossing is in addition accompanied by a steep jump in Δ . Unavailable in conventional SPR measurements, the jump in Δ brings even higher sensitivity when quantitatively characterizing the growing film.²⁴ Indeed, Tab. 3 confirms that using the information on Δ , about 3-4 times weaker concentrations of analyte can be detected than using Ψ . Of course, higher

absolute response does not guarantee higher sensitivity – one must take into account the noise level. For rotating analyzer measurements with auto-retarder the uncertainty in the Fourier coefficients propagates to absolute error in Δ about twice larger than in Ψ . In our measurements, the net increase in $\bar{\Delta}$ is higher than this factor (cf. Fig. 6), confirming the higher sensitivity of this ellipsometric angle to the growing film. Using rotating compensator the situation becomes more complicated, but the results of error propagation are similar.²⁵ Under favorable conditions, the net improvement of sensitivity coming from using Δ is reported to reach an order of magnitude.²⁶

The SPR resonance structure dominates both reflectivity and ellipsometric spectra. In conventional SPR second derivative can be used to numerically enhance the sensitivity of the measurement through SPR dip narrowing,²⁷ the ellipsometric data allow, however, for more efficient processing using the difference spectra peaks. Together with the fact that $\Delta - \Delta_0$ attains its maximum near the resonance, $\bar{\Delta}_{\max}$ can be favored for the use as a single-value description of growing layer. Analyzing reliability of $\Psi - \Psi_0$ and $\Delta - \Delta_0$ we have shown that realistic conditions of the experiment must be followed in numerical simulations when approaching the perfect resonance. Our findings are in agreement with the reported fact that in SPR measurements, large errors can cause small consequences.²⁸

Binding effectivity curves. Despite testing various constructs and concentrations (cf. Tabs. 1, 2) of CTD to immobilize, $\bar{\Psi}_{\max}$ and $\bar{\Delta}_{\max}$ in Fig. 7 align strikingly along sigmoidal curves, even compared to individual difference spectra in Fig. 6, which yet show no organization themselves. This suggests that one can use the concept of available residues to estimate the windows of concentration and flow speed needed for a generic TIRE binding experiment to provide usable results.

Our treatment starts from the asymptotic value A (cf. Tab. 3), which poses the lower bound c_{\min} on the detectable concentration. As Fig. 7 suggests, the flow speed must be adjusted so that c_{\min} falls into the noise-limited resolving power of the equipment (of course, particular values of A depend on the cell geometry).

Subsequently, the value of M appoints the concentration of analyte, at which the measurement response is steepest. Although M is often used also as an estimate of K_d , the discrepancy between M in Fig. 8 and direct fitting of the exponentials in Fig. 9 confirms that ellipsometric response to the concentration of the analyte is nonlinear. According to expectation, in agreement with NMR data for (unphosphorylated) CTD²⁹ is the directly fitted value of K_d in Tab. 5. Further, monitoring of M (e.g. in Tab. 3) can be used to restrict the mass-transfer limitation.³⁰ This is highly desirable since once the binding curves flatten, the available remedies (increasing flow speed and/or decreasing analyte concentration) contradict sensitive detection.

Practical benefits. Although measurement of full spectra during injection is impractical, a dozen wavelengths can be dynamically monitored without need to interrupt the injection. In the CID binding phase of our experiment we have demonstrated that such dynamical scans are completely

sufficient to construct the binding effectivity curves (see Fig. 9). Since several wavelengths around the background resonance are usually monitored anyway, the advanced analysis that we suggest here can readily be incorporated into current measurement practice. Actually, as the data already exist in many cases, the binding effectivity can be analyzed even retrospectively.

Also, usually there is an obstacle in comparison of spectra taken at different substrates, where the resonance positions unavoidably disagree. With difference spectra this can be corrected in a natural way: using the wavelength relative to background resonance frequency (cf. Fig. 6) the difference spectra from different substrates become conveniently aligned.

Conclusions

We have successfully demonstrated that in SPR-enhanced spectroscopic ellipsometry one can avoid the need of explicit knowledge on the SPR substrate when working with difference spectra of the ellipsometric angles. The basic advantage of the difference spectra resides in obtaining single peak footprint of the forming layer, which facilitates its robust and sensitive detection. For low concentrations, the difference spectrum in Δ is clearly to be favored. Finally, aligning properly the horizontal axis, the difference spectra from different chips can be aligned in a natural way. A good quantitative measure of difference spectra reliability is the error of their linear approximation (7) or, when quick reference suffices, Fig. 5.

Using RNAPII-CTD of various length and concentration, we have for the immobilization stage of a TIRE experiment reliably quantified the influence of channel flow speed. The obtained binding effectivity curves can be used in scheduling a generic TIRE experiment. For the binding stage of the experiment we have successfully confirmed the ability of the SPR-TIRE setup to detect the weak ($K_d \approx 10^{-3}$ M) protein-protein interaction of the CTD and Rtt103-CID.

The advantage of the suggested treatment resides in the fact that it can be easily incorporated into current day measurement practice.

Acknowledgements

This work was supported by the projects "CEITEC - Central European Institute of Technology" (CZ.1.05/1.1.00/02.0068) from European Regional Development Fund, TWINFUSYON (GA692034) and by Czech Science Foundation (GA15-24117S). Group of dr. Štefl is acknowledged for providing the samples of CTD and Rtt103.

Appendix

We use the PVD deposited Au on Cr wetted BK7 glass chips, with the nominal Au layer thickness of 40 nm. During measurement, the chip was coupled to the half-cylinder shaped BK7 prism using index matching oil ($n_d = 1.51$) to minimize the light losses and distortion. Each TIRE chip contains three independent channels, and each channel was used for a single measurement without reuse.

Prior to measurements, the chips were washed in ethanol and SAM1 was incubated for 18 hours by complete

submersion of the chip in 1 mM ethanol solution of 6-amino-1-hexanethiol (purchased from Sigma-Aldrich). Directly after incubation of SAM1, the chip was washed with ethanol and then with DI water and placed into a humid chamber for one hour to incubate SAM2 from droplet of 4% grade II glutaraldehyde water solution (Sigma-Aldrich) covering the gold area of the surface. Directly after incubation, the chip was washed in DI water, placed into the TIRE cell and flushed with buffer. The final glutaraldehyde layer is well suited to interact with various amino groups of CTD.³¹

To cross check the results, we have used two groups of self-synthesized CTD: four heptapeptide repeats (E2 XY, see below) and thirteen heptapeptide repeats (E213fl and E513fl, see below).

The first group of peptides has been based on the E2 structure, a FLAG-tagged four repeats (labelled according to N-terminus-ABCD-C-terminus) of the CTD motive, YSPTSPS, in overall length of 49 residues, E2 = SPEFTCSPS (YSPTSPS)₄ YAAADYKDDDDK. The peptides E2 XY available in this experiment were modified during production through exchanging the second serine with glutamate (S₂ → E) in various combinations of modified repeat X and Y: (unmodified) E2 (2.45 mM), E2 C (1.76 mM), E2 CD (2.2 mM), E2 AB (2.0 mM).

The second group of peptides has been based on E13 structure, a FLAG-tagged thirteen repeats of the CTD motive, in overall length of 117 residues, E13 = SPEFTCSPTPEPS (YSPTSPS)₁₃ YSPAAADYKDDDDK. The available peptides E213fl (0.96 mM) and E513fl (lyophilized from 200 μl of 0.7 mM solution) were modified (S → E) on all second and all fifth serines, respectively.

All available CTD peptide stock solutions were in ITC buffer (35 mM KH₂PO₄, 100 mM KCl, 1 mM BME, pH 6.8). Prior to measurement, all stock solutions were diluted approx 1:4 (100 μl of peptide stock solution in 400 μl of ITC buffer). The measured E513fl solution was obtained by dissolving all the available amount of the peptide in 500 μl of the ITC buffer. The resulting concentrations of peptides used in measurement are summarized in Tabs. 1, 2.

The 142 residues long CTD interacting domain, CID, of the Rtt103 protein, Rtt103-CID, 350 μM in ITC buffer, was used in the binding experiment. The actual concentrations used in the experiment were full stock concentration (design. 1/1) and its twofold step dilutions 1/2, 1/4 and 1/8. For information on structure of the Rtt103-CID domain see Fig. 10 and²⁹.

The conventional estimate on sizes of all molecules involved in our experiment indicates that the resulting (mono)layers over the TIRE chip are very thin: about 1 nm for each of the SAMs (from bond lengths), at most 20 nm for E2 and 40 nm for E213 and E513 modifications (in unstructured form); the size of Rtt103-CID is about 3x4x5 nm³ (from alpha helix pitch). All the sizes are well below the visible light wavelength.

References

1. S.A. Maier. Plasmonics: Fundamentals and Applications. Springer, 2007.
2. J. Homola. "Present and future of surface plasmon resonance". Anal Bioanal Chem. 2003. 377: 528-539.

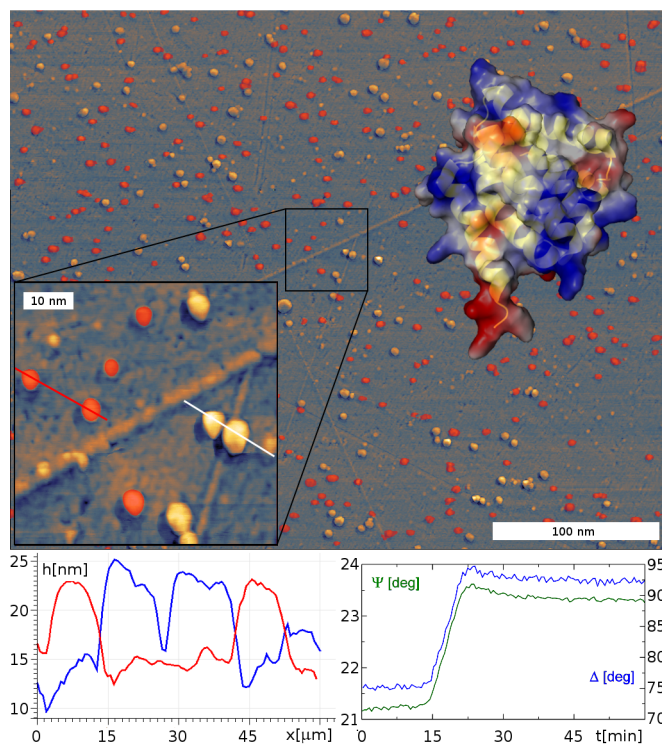


Figure 10. AFM phase-contrast image of Rtt103-CID directly immobilized over SiO₂/Au substrate using the TIRE system (upper panel). The egg-shaped structure of the protein is enlarged within the upper right inset (the surface charge is estimated using `pymol` software with blue for positive). The candidates for Rtt103-CID, complying with dimensions deduced from rcsb.org 2KM4 structure, are masked red. Lower panels: the height profiles (left) from the positions marked in the lower-left inset of the main figure and TIRE monitoring of Rtt103-CID binding to the chip (right).

3. H.G. Tompkins, E.A. Irene, editors. Handbook of ellipsometry. Springer, 2005.
4. Arwin H., Poksinski M., Johnsen K.. "Total internal reflection ellipsometry: principles and applications". Applied Optics. 2004. 43(15): 3028-3036.
5. S.G. Nelson, K.S. Johnston, S.S. Yee. "High sensitivity surface plasmon resonance sensor based on phase detection". Sensors and actuators B. 1996. 35-36: 187-191.
6. S.Patskovsky, M. Meunier, A.V. Kabashin. "Phase sensitive silicon-based total internal reflection sensor". Optics Express. 2007. 15(19).
7. T. Isoniemi, S.Tuukkanen, D.C. Cameron, J. Simonen and J. Toppari. "Measuring optical anisotropy in poly(3,4-ethylene dioxothiophene):poly(styrenesulfonate) films with added graphene". Organic electronics. 2015. 25: 317-323.
8. H.A. Engström, P.O. Andersson, S. Ohlson. "A label-free continuous total-internal-reflection-fluorescence-based immunosensor". Analytical Biochemistry. 2005. 357(2).
9. I. Baleviciute et al. "Study of antibody/antigen binding kinetics by total internal reflection ellipsometry". Biosensors and Bioelectronics. 2013. 39(1).
10. T. Kang, Y. Niu, G. Jin. "Visualization of the interaction between tris and lysozyme with a biosensor based on total internal reflection imaging ellipsometry". Thin Solid Films. 2014. 571: 463-467.

11. S. Ekgasit, Ch. Thammacharoen, F. Yu and W. Knoll. "Influence of the Metal Film Thickness on the Sensitivity of Surface Plasmon Resonance Biosensors". *Applied Spectroscopy*. 2005. 59(5): 661-667
12. M.-L. Thève. "Investigation of the Optical Properties of Au by Means of Thin Semitransparent Films". *Phys. Rev. B*. 1970. 2(8): 3060-3078.
13. D.E. Aspnes, E. Kinsbron, D.D. Bacon. "Optical properties of Au: Sample effects". *Phys. Rev. B*. 1980. 21(8): 3290-3299.
14. M. Koenig, T. Kasputis, D. Schmidt et al. "Combined QCM-D/GE as a tool to characterize stimuli-responsive swelling of and protein adsorption on polymer brushes grafted onto 3D-nanostructures". *Anal Bioanal Chem*. 2014. 406:7233-7242.
15. D. Aspnes. "Optical approaches to the Determination of Composition of Semiconductor Alloys During Epitaxy". *IEEE J. Sel. Top. Quant. Elect*. 1995. 1(4): 1054-1063.
16. E. Hecht. "Optics". Addison-Wesley. 2001.
17. E.D. Palik, ed. "Handbook of optical constants of solids". New York: Academic Press, 1985. Vol. 1, 286-295.
18. D. Roy. "Surface Plasmon Resonance Spectroscopy of Dielectric Coated Gold and Silver Films on Supporting Metal Layers: Reflectivity Formulas in the Kretschmann Formalism". *Applied Spectroscopy*. 2001. 55(8): 1046-1052.
19. Y.W. Jung et al. "Study of the Interaction Between HSA and Oligo-DNA Using Total Internal Reflection Ellipsometry". *JOURNAL OF THE KOREAN PHYSICAL SOCIETY*. 2012. 60(8): 1288-1291.
20. Y.R. Kang et al. "Monitoring of the Binding Between EGFR Protein and EGFR Aptamer Using In-Situ Total Internal Reflection Ellipsometry". *J. Nanosci. Nanotechnol*. 2016. 60(6): 6445-6449
21. N. Li, H.H. Nguyen, M. Byrom, A.D. Ellington. "Inhibition of Cell Proliferation by an Anti-EGFR Aptamer". *PLoS ONE* 6(6): e20299. 2011.
22. A. Meinhart, P. Cramer. "Recognition of RNA polymerase II carboxy-terminal domain by 3'-RNA-processing factors". *Nature*. 2004. 430: 223-226.
23. W-H. Tsai, Y-C. Tsao et al. "Cross-point analysis for a multimode fiber sensor based on surface plasmon resonance". *Opt. Lett*. 2005. 30(17): 2209-2211.
24. Z. Balevicius, I. Baleviciute et al. "In situ study of ligand-receptor interaction by total internal reflection ellipsometry". *Thin Solid Films*. 2014. 571: 744-748.
25. R. Kleim, L. Kuntzler, A. El Ghemmaz. "Systematic errors in rotating-compensator ellipsometry". *J. Opt. Soc. Am*. 1994. 11(9): 2550-2559
26. A. Nabok, A. Tsargorodskaya. "The method of total internal reflection ellipsometry for thin film characterisation and sensing". *Thin solid films*. 2008. 516(24): 8993-9001.
27. A. Ikehata, K. Ohara, H. Shinzawa and Y. Ozaki. "Sensitive Detection and Identification of Organic Liquids Using the Second Derivative of Surface Plasmon Resonance Near-Infrared Spectra". *Applied Spectroscopy*. 2008. 62(5): 517-524
28. A. Rueda, N. Vogel, M. Kreiter. "Characterization of gold films by surface plasmon spectroscopy: Large errors and small consequences". *Surf. Sci*. 2012. 603: 491-497.
29. B.M. Lunde et al. "Cooperative interaction of transcription termination factors with the RNA polymerase II C-terminal domain". *Nat Struct Mol Biol*. 2010. 17(10): 1195-1201.
30. R.W. Glaser. "Antigen-antibody binding and mass transport by convection and diffusion to a surface; a two-dimensional computer model of binding and dissociation kinetics". *Analytical Biochemistry*. 1993. 213(1): 152-161.
31. I. Migneault, C. Dartiguenave et al. "Glutaraldehyde: behavior in aqueous solution, reaction with proteins, and application to enzyme crosslinking". *BioTechniques*. 2004. 37(5): 790-802.